Computational Study for Reactions of H Atoms with Adsorbed SiH3 and Si2H5 on H-Covered Si(100)-(2×1) Surface

ARTICLE *in* THE JOURNAL OF PHYSICAL CHEMISTRY C · SEPTEMBER 2014

Impact Factor: 4.77

2 AUTHORS, INCLUDING:

Hsin-Tsung Chen

Chung Yuan Christian University

78 PUBLICATIONS **703** CITATIONS

THE JOURNAL OF PHYSICAL CHEMISTRY C

Article

pubs.acs.org/JPCC

Computational Study for Reactions of H Atoms with Adsorbed SiH_3 and Si_2H_5 on H-Covered Si(100)-(2 × 1) Surface

Hsin-Tsung Chen* and Hsien-Wei Huang

Department of Chemistry and Center for Nanotechnology, Chung Yuan Christian University, Chungli 32023, Taiwan

Supporting Information

ABSTRACT: Density functional theory calculations with spin-polarization effect were employed to illustrate the adsorption of Si_xH_y (x = 1−2; y = 1−5) species and the reactions of H atoms with adsorbed SiH_x (x = 1−3) and Si_2H_5 species on the H-covered Si(100)-(2 × 1) surface. The configurations and energies of these adsorbates were elucidated. It was found that H vacancy sites can be easy created by SiH_3 and Si_2H_5 radicals with small barriers (2.1 and 1.6 kcal/mol for SiH_3 and Si_2H_5, respectively). The Si_2H_5, Si_2H_4, $SiHSiH_3$, SiH_3, SiH_2, SiH, and Si radials interact with the surface more forcefully than the Si_2H_6 and SiH_4 molecules. Potential energy surfaces for the reaction mechanisms of H + SiH_x(a) and H + Si_2H_5(a) were mapped by using the nudged elastic band method. The calculation results demonstrate that the most favorable pathway is hydrogen abstraction leading to the production of H_2 and Si_xH_y (x = 1−2; y = 0−4) because of their low barriers and high exothermicities. Rate constant calculations were performed to study the kinetic behavior for simulation of silicon thin-film growth by chemical vapor deposition processes.

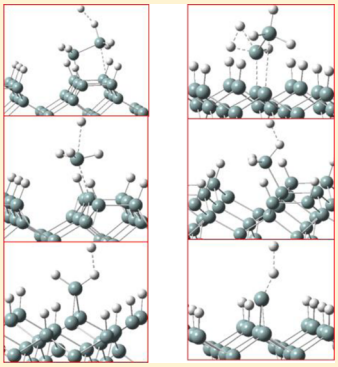

INTRODUCTION

In recent decades, silicon chemical vapor deposition (CVD) processes, such as plasma-enhanced CVD (PECVD), catalytic CVD (Cat-CVD), and thermal CVD[1−7] have been generally employed for producing hydrogenated amorphous silicon (a-Si:H), polycrystalline silicon (p-Si), and silicon nitride (SiN_x) films at low-temperature ranges in the semiconductor industry. Among these methods, PECVD is a high potential and extensive technique for yielding a uniform high-quality silicon thin film on a large-scale substrate.[1] These promising films have been applied to thin film transistors (TFTs) for active-matrix liquid crystal displays, multijunction solar cells, light emitting diodes, photoreceptors, active pixel image sensors, and sensing devices.[8−11] Si film growth by the CVD processes includes two reaction process regimes, the gas-phase and the gas−surface reaction processes. The probability of each molecule gas−surface reaction determines the importance as a precursor for thin film growth. Source gases are dissociated by collisions with high-energy electrons in gas discharge plasmas in the PECVD method, whereas those are decomposed by the catalytic cracking process with a glowing high-temperature catalyst in the Cat-CVD method. These species (molecules, atoms, radicals, and ions) undergo secondary reactions in the gas phase and then diffuse onto the substrate, depositing an a-Si:H film through surface reaction processes. The identification of precursors is clearly desirable to exactly control the properties of the Si thin film.[12]

Silane (SiH_4) and disilane (Si_2H_6) have been used as thin-film precursors[1,13−15] in industry, dopant precursors in III−V composite semiconductors, and in deposition of epitaxial layers of Si,[16,17] $Si_{1-x}Ge_x$,[18,19] and SiC.[20] A well-established mechanism is the dissociation of the SiH_4 and Si_2H_6 species into Si_xH_y (x = 1−2; y = 1−5) fragments resulting in Si thin-film growth with release of hydrogen atoms and molecules.[21−32] However, abundant hydrogen atoms in the gas phase can further react with the adsorbed Si_xH_y species by hydrogen-abstraction and addition−elimination processes, giving different pathways as follows:

$$H(g) + Si_2H_5(a) \rightarrow H_2(g) + Si_2H_4(a) \quad (R1)$$

$$\rightarrow H_2(g) + SiHSiH_3(a) \quad (R2)$$

$$\rightarrow SiH_4(g) + SiH_2(a) \quad (R3)$$

$$\rightarrow 2SiH_3(a) \quad (R4)$$

$$\rightarrow Si_2H_6(g) \quad (R5)$$

$$H(g) + SiH_3(a) \rightarrow SiH_4(g) \quad (R6)$$

$$H(g) + SiH_3(a) \rightarrow H_2(g) + SiH_2(a) \quad (R7)$$

$$H(g) + SiH_2(a) \rightarrow H_2(g) + SiH(a) \quad (R8)$$

$$H(g) + SiH(a) \rightarrow H_2(g) + Si(a) \quad (R9)$$

The gas−surface physical-chemical reaction processes in Si_xH_y/H_2 plasmas are very complicated. A mechanistic understanding of these processes is vital for modeling silicon CVD chemistry. In general, detailed understanding of these reaction mechanisms is very difficult under very limited experimental conditions. Kubo et al. have used tight-binding quantum chemical molecular dynamics to simulate silicon crystal growth

Received: May 10, 2014
Revised: August 12, 2014
Published: August 14, 2014

   dx.doi.org/10.1021/jp504612g | J. Phys. Chem. C 2014, 118, 20314−20322

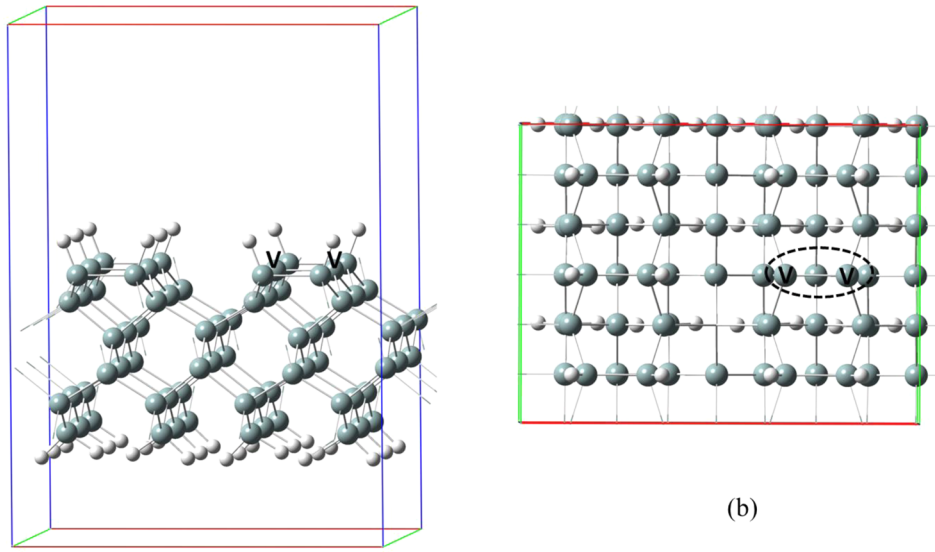

Figure 1. (a) Side view and (b) top view of the H-covered Si(100)-(2 × 1) surface with two H vacancy sites. V represents the H vacancy sites.

mechanisms for deposition of SiH_3 and SiH_2 radicals on the H-terminated Si(001) in a CVD process.[33,34] Maroudas et al. reported several detailed studies on the hydrogen-induced crystallization mechanisms of amorphous silicon thin film via molecular dynamics (MD) simulations.[35−37] Montalenti also showed hydrogen atoms can promote growth of ordered and epitaxial Si thin films in PECVD at low temperature on the H-terminated Si(001)-(2 × 1) by employing Car−Parrinello simulations and static density functional theory (DFT) calculations.[38] In addition, DFT calculations have provided a way to obtain the electronic adsorption structures and the silicon-related reaction mechanisms accurately.[39−43] In this work, we study the detailed mechanisms of the reactions of H atoms with adsorbed SiH_x (x = 1−3) and Si_2H_5 species and predict the rate constants for the mentioned reactions by means of DFT calculations and transition-state theory (TST).

COMPUTATIONAL DETAILS

Geometric optimizations for all structures presented in this paper are performed with the DFT calculations as implemented in the Vienna ab initio simulation package (VASP).[44−47] The Perdew−Burke−Ernzerhof (PBE)[48] form for the generalized gradient approximation (GGA) exchange correlation functional with a plane wave basis set is carried out during the calculations. For the Brillouin zone integration, a Monkhorst−Pack (3 × 3 × 1) k-points grid is applied. The cutoff energy is set at 300 eV and converges to 0.01 eV in total energy. Spin-polarization effects are considered for the radicals during the calculations.

As shown in Figure 1, the H-covered Si(100) periodic slab is modeled in a $p(2 \times 1)$ later cell with six atomic Si layers, and each layer contains 12 silicon atoms. The top Si layer of the surface is covered by hydrogen atoms and the bottom one is terminated by hydrogen atoms forming symmetric SiH_2 groups. A vacuum gap greater than 10 Å is introduced in the direction perpendicular to the surface. The bottom three silicon layers are constrained at the bulk parameters, while the remaining layers are fully optimized. Previous studies have demonstrated that the supercell used in this work is sufficient for modeling the silicon surface.[39,49,50] It should be noted that we also performed test calculations for SiH_3 and Si_2H_5 adsorption on six-, seven- and eight-layer Si(100) surfaces. The difference (less than 1.0 kcal/mol) of the adsorption energy can be neglected. In addition, we also performed a similar calculation for SiH_3 and Si_2H_5 adsorption on (2 × 1), (2 × 2), and (3 × 1) surfaces. The effect of the supercell size is ignored because of the small relative energy (<1.0 kcal/mol). Thus, the Si(100)-(2 × 1) surface with six-layer atomic silicon is sufficient to explore the adsorption and reactions of H atoms with adsorbed SiH_x and Si_2H_5.

The adsorption energy of a adsorbate can be computed as described in a previous study[40] as follows:

$$E_{ads} = E_{mole/surface} - (E_{mole} + E_{surface})$$

where E_{mole}, $E_{surface}$, and $E_{mole/surface}$ are the energy of an Si_xH_y molecule, the energy of a H-covered Si(100)-(2 × 1) surface, and the energy of the Si_xH_y molecule adsorbed on the surface, respectively. Notice that a negative E_{ads} value represents stable adsorption.

The minimum energy paths (MEPs) and transition structures (TSs) between reactants, intermediates, and products for the reactions of H(g) + Si_2H_5(a) and H(g) + SiH_x(a) are obtained by the nudged elastic band (NEB) method.[51,52] At least eight images between the reactant state and product state are used to interpolate the reaction pathway and locate the TS. The frequency calculations are performed to verify the transition state. Rate constants for the above-mentioned reactions are estimated by empolying the transition-state theory.[53]

RESULTS AND DISCUSSION

To confirm the validation of the calculation results, we first compared the heat of reactions (ΔH) for some decomposition reactions in the gas phase. For the gas-phase calculation, a periodic array of each molecule in a 20 × 20 × 20 Å^3 cubic supercell was carried out. The used lattice size is large enough to neglect the interaction between the molecule and its repeated images. Table 1 shows the comparison of the calculated and experimental ΔH of H + Si_2H_5 and H + SiH_3

dx.doi.org/10.1021/jp504612g | J. Phys. Chem. C 2014, 118, 20314−20322

Table 1. Calculated and Experimental Heat of Reactions of H + Si_2H_5 and H + SiH_3

reaction		ΔH (kcal/mol) spin	non_spin	exptl
H + Si_2H_5 →	Si_2H_6	−86.7	−118.6	−89.3
	SiH_2 + SiH_4	−28.4	−62.9	−38.2
	SiH_3+SiH_3	−11.9	−25.5	−12.6
	H_2 + Si_2H_4	−35.8	−70.2	−47.0
	H_2 + $SiHSiH_3$	−16.5	−61.7	–
H + SiH_3 →	SiH_4	−89.8	−125.5	−89.9
	H_2 + SiH_2	−28.0	−63.7	−35.1

with and without considering the spin-polarization effect for the radial molecules. The different energies of ΔH between the spin-polarization calculation and experiment are small (within 0.1−11.2 kcal/mol) by comparison with those (within 12.9−35.6 kcal/mol) without considering spin-polarization effect. Accordingly, the calculation results considering the spin-polarization effect are better in agreement with the experimental results[54,55] than those without the spin-polarization cases. All the radicals' calculations were consequently optimized with the spin-polarization effect. For the SiH_4 structure, the predicted Si−H bond distance, 1.502 Å, closely agrees with the experimental value of 1.481 Å.[56] For Si_2H_6 configuration, the predicted bond distances of Si−H, Si−Si, and the angle of HSiSi (1.507 Å, 2.340 Å, and 110.1°, respectively), are well in agreement with the experimental data of 1.486 Å, 2.327 Å, and 111.0°.[56] Furthermore, the lattice constant is calculated to be 5.47 Å, which is consistent with the experimental value of 5.43 Å.[57]

Adsorption of Si_2H_6, Si_2H_5, Si_2H_4, $SiHSiH_3$, SiH_4, SiH_3, SiH_2, SiH, and Si on the H-covered Si(100)-(2 × 1) Surface. To investigate the reactions of an H atom with adsorbed SiH_3 and Si_2H_5, we first study the adsorption of Si_2H_6, Si_2H_5, Si_2H_4, $SiHSiH_3$, SiH_4, SiH_3, SiH_2, SiH, and Si on the H-covered Si(100)-(2 × 1) surface. The interactions between these species and the surface are critical and require detailed understanding because they take place in the initial growth stages. Adsorption of SiH_3 and Si_2H_5 radicals will not take place on the fully H-covered Si(100)-(2 × 1) surface, requiring surface dehydrogenation to create reactive H vacancy sites and dangling bonds. The dangling bonds on the Si(100)-(2 × 1) surface are passivated when the concentration of hydrogen atoms is high. Removal of H atoms from the surface is needed to form the reactive adsorption sites and dangling bonds. Maroudas et al. have studied H-abstraction reaction by H(D)[58,59] and SiH_3 radicals[60−62] from hydrogen-terminated Si(100)-(2 × 1) surface by performing MD simulations. Their MD simulations using a Si-cluster model agree well with DFT calculations. In addition, they also showed SiH_3 radicals can insert into strained Si−Si bonds without any barrier by using first-principles calculations.[63] We have shown that hydrogen abstraction reaction takes place first to produce the dangling bonds and can be described as

$$SiH_3(g) + H(s) \rightarrow SiH_4(g) + \text{H-covered surface with one vacancy} \quad \text{(I)}$$

$$Si_2H_5(g) + H(s) \rightarrow Si_2H_6(g) + H(s) - \text{surface} + \text{one vacancy} \quad \text{(II)}$$

The activation barriers and reaction energies for the abstraction reactions (reaction I) are calculated to be 2.1 and −8.7 kcal/mol, while those are 1.6 and −8.3 kcal/mol for reaction II. The results agree well with other calculation results (activation barrier and reaction energy are ∼2.08 kcal/mol and −5.77 to −8.07 kcal/mol, respectively) for the abstraction reaction of $SiH_3(g)$ + H(s).[64,65] Our calculations show that it is easy to create the vacancy sites and the dangling bonds on the fully H-covered Si(100)-(2 × 1) surface because of the low abstraction barriers. As expected, the dangling bonds exhibit high active sites to react with the species of Si_2H_6, Si_2H_5, Si_2H_4, $SiHSiH_3$, SiH_4, SiH_3, SiH_2, SiH, and Si. Their optimized geometries are depicted in Figure 2. The related adsorption energies are summarized in Table 2.

SiH_4 and Si_2H_6 Adsorption. The adsorption energies and optimized configurations of Si_2H_6 and SiH_4 are found in Table 2 and Figure 2. As shown in Figure 2, the Si_2H_6 and SiH_4 molecules can interact with a Si atom of the dangling bond by physisorption, utilizing theirs H atoms. The distances of H···

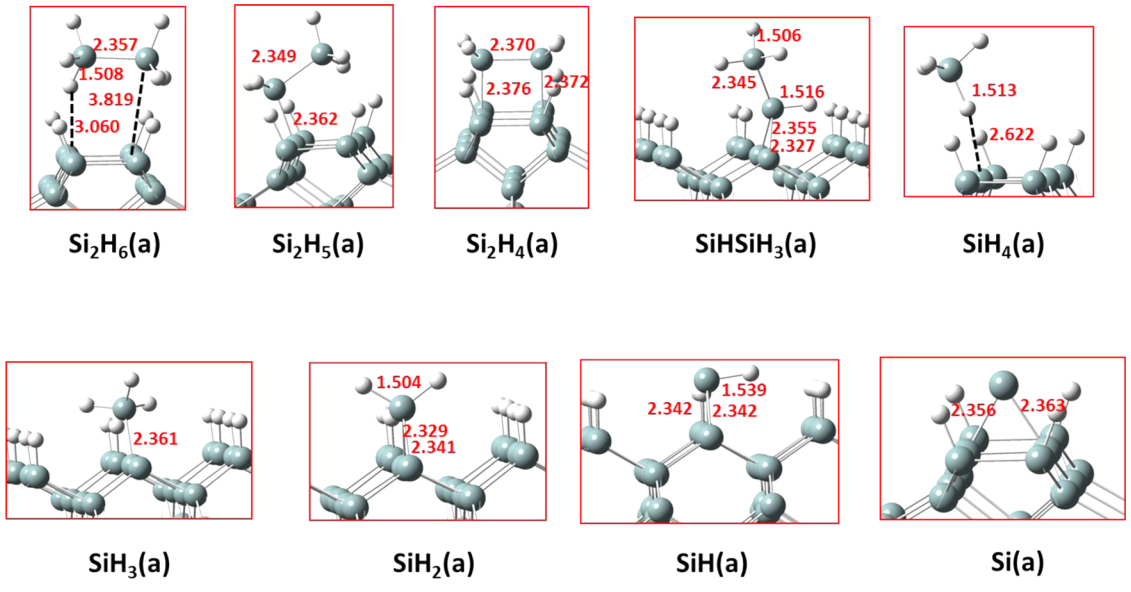

Figure 2. Optimized geometries of Si_2H_6, Si_2H_5, Si_2H_4, $SiHSiH_3$, SiH_4, SiH_3, SiH_2, SiH, and Si on the H-covered Si(100)-(2 × 1) surface.

dx.doi.org/10.1021/jp504612g | J. Phys. Chem. C 2014, 118, 20314−20322

Table 2. Adsorption Energies (Kilocalories per Mole) of Si_2H_6, Si_2H_5, Si_2H_4, $SiHSiH_3$, SiH_4, SiH_3, SiH_2, SiH, and Si on the H-Covered Si(100)-(2 × 1) Surface

species/adsorption site	H-covered surface	clean surface
Si_2H_6	−0.08	
Si_2H_5	−63.7	−54.2
Si_2H_4	−94.2	−84.6
$SiHSiH_3$	−82.9	
SiH_4	−0.06	
SiH_3	−65.5	−55.8
SiH_2	−86.0	−77.0
SiH	−86.9	
Si	−88.1	

Si(s) are 3.060 and 2.622 Å, respectively. The Si−Si bond distance of the Si_2H_6 adsorption and Si−H bond length of the SiH_4 adsorption are 2.357 and 1.513 Å, which are slightly longer than those at gas phase (2.340 and 1.502 Å). Their adsorption energies are predicted to be −0.08 and −0.06 kcal/mol for the Si_2H_6 adsorption and the SiH_4 adsorption, respectively. Because of the small adsorption energy, the Si_2H_6 and SiH_4 are assigned to weak molecular adsorption on the surface and connecting to chemisorbed species.

Si_2H_5, Si_2H_4, $SiHSiH_3$, SiH_3, SiH_2, SiH, and Si Adsorption. Similar to the adsorption of Si_2H_6 and SiH_4, we examined the most stable adsorption structures and energies for their derivatives, Si_2H_5, Si_2H_4, $SiHSiH_3$, SiH_3, SiH_2, SiH, and Si on the H-vacancy sites of the H-covered Si(100)-(2 × 1) surface for following mechanistic studies. All located lowest-energy adsorbed states of Si_2H_5(a), Si_2H_4(a), $SiHSiH_3$(a), SiH_3(a), SiH_2(a), SiH(a), and Si(a) are given in Figure 2. The adsorption energies of those derivatives are summarized in Table 2. As one could expect, the Si_2H_5, $SiHSiH_3$, SiH_3, SiH_2, SiH, and Si radicals interact with the surface more strongly than the closed-shell Si_2H_6 and SiH_4 molecules do. The most stable Si_2H_5 adsorption is found at a Si site of the dangling bond with an adsorption energy of −63.7 kcal/mol. The Si−Si bond distance of the Si_2H_5(a) is 2.349 Å, and the forming Si−Si(s) bond length is 2.362 Å. The most stable $SiHSiH_3$ adsorption is bidentate at two Si sites of the dangling bond with an adsorption energy of −82.9 kcal/mol. The Si−Si bond distance of the $SiHSiH_3$(a) is 2.345 Å, and the two forming Si−Si(s) bond distances are 2.355 and 2.327 Å. The SiH_3 bonds with one Si site of the dangling bond with an adsorption energy of −65.5 kcal/mol and the forming length of the Si−Si(s) bond is 2.361 Å. For the SiH_2 adsorption, the most stable configuration is located at the Si(s), Si(s) bridging site of the dangling bond. The adsorption energy of the bidentate SiH_2(a) is calculated to be −86.6 kcal/mol. The Si atom of the SiH_2(a) is bound to two Si atoms of the surface with Si−Si(s) distances of 2.329 and 2.341 Å. Similar to SiH_2, the SiH and Si preferentially adsorb on the bridging site of the surface, forming SiH(a) and Si(a), respectively. As listed in Table 2, the adsorption energies of SiH(a) and Si(a) are −86.9 and −88.1 kcal/mol, respectively. While the corresponding distances for the Si−Si(s) bonds are 2.342 and 2.342 Å for the SiH(a) and 2.356 and 2.363 Å for the Si(a), respectively. For the other closed-shell Si_2H_4 molecule, the adsorption energy is computed to be −94.2 kcal/mol. It suggests that disilene is highly reactive with the H-covered surface. The optimized configurations of Si_2H_4 adsorption resembles the C_{2v} structure of the stable Si_2H_4 structures, which is agreement with that reported by Kohler er al.[66] The Si−Si

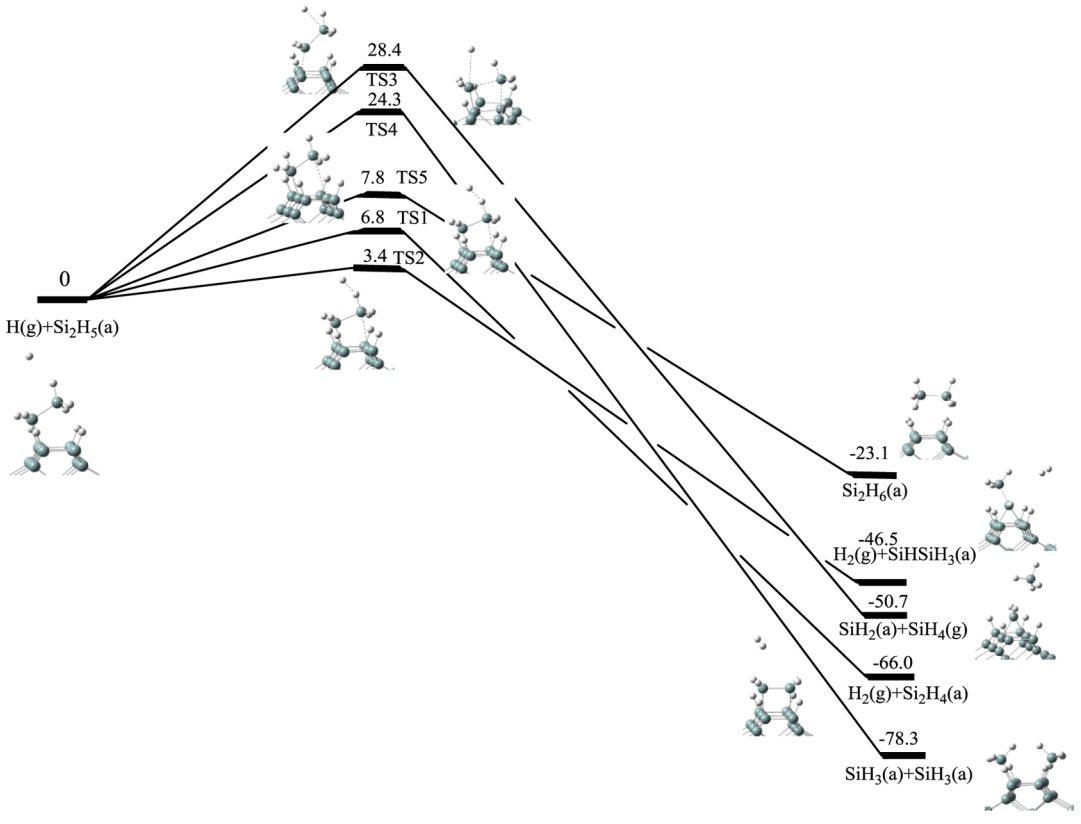

Figure 3. Schematic potential energy profiles for the reaction of H + Si_2H_5(a) on the H-covered Si(100)-(2 × 1) surface.

dx.doi.org/10.1021/jp504612g | J. Phys. Chem. C 2014, 118, 20314−20322

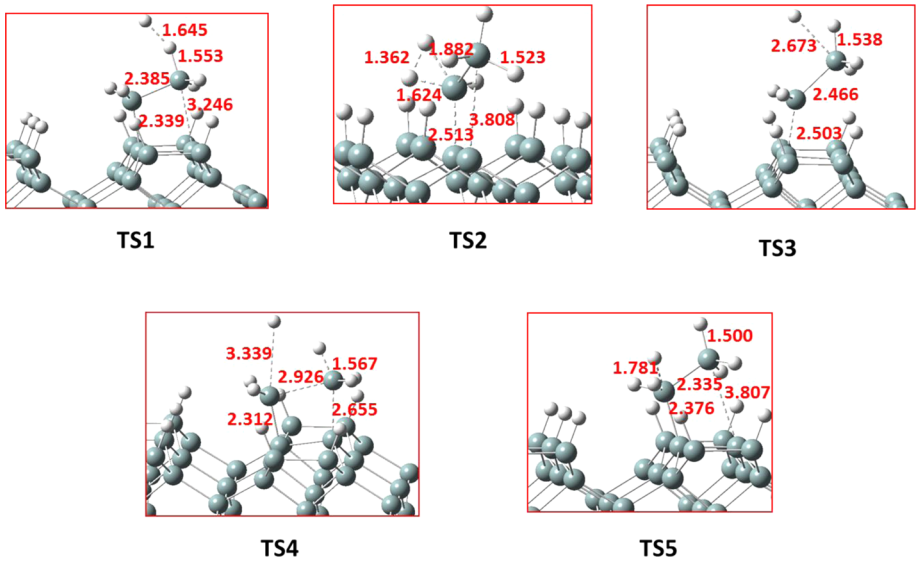

Figure 4. Optimized geometries of transition states for the reaction of H + Si_2H_5(a).

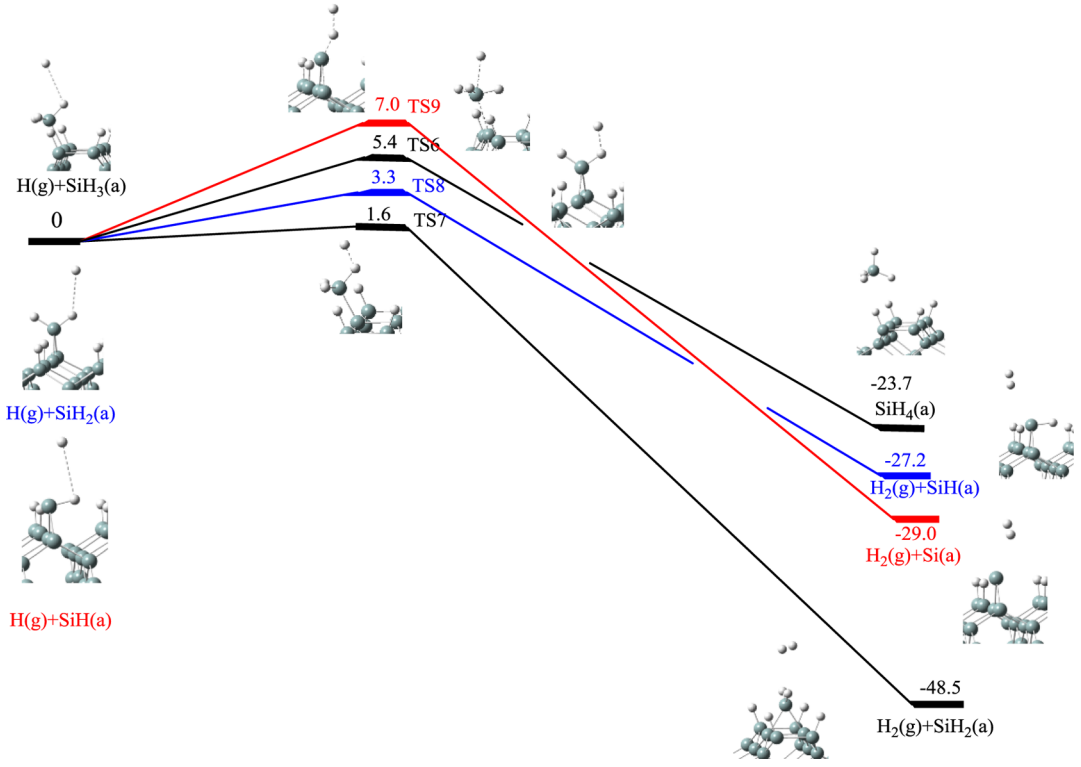

Figure 5. Schematic potential energy profiles for the reaction of H + SiH_x(a) (x = 1−3) on the H-covered Si(100)-(2 × 1) surface.

bond distance of the Si_2H_4(a) is 2.370 Å, and the forming Si−Si(s) bond distances are 2.372 and 2.376 Å.

In addition, we also compare the adsorption energies of some species on the H-covered Si(100) surface and on the clean Si(100) surface. As shown in Table 2, the calculated adsorption energy with hydrogen coadsorption on the surface increases in the range of 10−11 kcal/mol. These results suggest that the hydrogen coadsorption may stabilize the Si_xH_y adsorption on the Si(100) surface. The enhancement effects of H coadsorption have been also demonstrated for OH,[67] HS,[68] NO_3,[69] and $HOBO_2$[70] species with titania surface, but not for SiH_x[71] on the TiO_2 anatase (101) surface.

Potential Energy Surface and Reaction Mechanism. *Reactions of Hydrogen Atom with Si_2H_5(a) on the H-Covered Si(100)-(2 × 1) Surface.* To investigate the basic reaction mechanism of Si_2H_5(a) with H(g) on the H-covered Si(100)-(2 × 1) surface, we mapped the potential energy surface (PES) of H(g) + Si_2H_5(a) on the surface by implementing the NEB method. For this reason, we have chosen the most stable adsorption of $SiHSiH_3$, Si_2H_4, SiH_3, SiH_2, and H. Five possible reaction pathways R1−R5 are considered for the interaction of Si_2H_5(a) with H(g) via H-abstraction and addition−elimination pathways, as alluded to in the introduction. The calculated PES for the reaction mechanisms of H(g) + Si_2H_5(a) is depicted in Figure 3. The full minimum-energy pathways for the reactions

dx.doi.org/10.1021/jp504612g | J. Phys. Chem. C 2014, 118, 20314−20322

of H(g) + Si_2H_5(a) as the function of proper reaction coordinate are represented in Figure S1 in the Supporting Information. All optimized configurations of transition states for the above reactions are given in Figure 4. As seen from Figure 3, all reactions are calculated to be exothermic with intrinsic barriers.

The first mechanism occurs by the attachment of the H atom at one of the hydrogens of part of SiH_3 in Si_2H_5(a) to produce the Si_2H_4(a) and H_2 via direct hydrogen abstraction reaction. The process is predicted to have an exothermicity of 66.0 kcal/mol and requires overcoming a 6.8 kcal/mol energy barrier at transition state TS1. The forming H···H and Si···Si(s) bond lengths are predicted to be 1.645 and 3.246 Å in TS1, respectively, while the rupturing H−Si bond distance is 1.553 Å. In the second direct hydrogen abstraction mechanism, the reaction happens by the attachment of the H atom at one of the hydrogens of the part of SiH_2 in Si_2H_5(a) to produce the $SiHSiH_3$(a) and H_2 via TS2. The forming H···H and Si···Si(s) bond lengths are computed to be 1.362 and 2.513 Å, while the rupturing H−Si bond distance is 1.624 Å. Furthermore, the exothermicity and barrier of this pathway are calculated to be 46.5 and 3.4 kcal/mol, respectively. The third channel is a SiH_4 abstraction mechanism and starts by the attachment of the H atom at the silicon atom of the part of SiH_3 in Si_2H_5(a) to produce the SiH_4(a) + SiH_2(a) by passing a highest barrier of 28.4 kcal/mol at TS3 with an exothermicity of 50.7 kcal/mol. The forming H···H and breaking Si−Si bond distances are 2.673 and 2.466 Å, respectively. The fourth pathway is an addition−elimination process and happens by the addition of a H atom at the silicon atom of the part of SiH_2 in Si_2H_5(a) to produce the SiH_3(a) + SiH_x(a) by passing the transition state TS4. The exothermicity and barrier of this process are calculated to be 78.3 and 24.3 kcal/mol, respectively. The forming H···Si and breaking Si−Si bond distances are predicted to be 3.339 and 2.926 Å, repsectively. The final process occurs by the addition of a H atom at the silicon atom of the part of SiH_2 in Si_2H_5(a) to produce the Si_2H_6(a) by passing the TS5 with an energy barrier of 7.8 kcal/mol and an exothermicity of 23.1 kcal/mol. The forming H···Si and Si−Si(s) bond distances are predicted to be 1.781 and 3.807 Å, respectively.

In summary, our calculations have shown that the hydrogen abstraction mechanism of the reaction H(g) + Si_2H_5(a) may dominate on the H-covered Si(100)-(2 × 1) surface because of its high exothermicity and low energy barrier.

Reactions of Hydrogen Atom with SiH_x(a) on the H-Covered Si(100)-(2 × 1) Surface. In this section, we describe the mechanism for the reaction of H(g) + SiH_x(a) based on the calculated PES presented in Figure 5. The full minimum-energy pathways for the reactions of H(g) + SiH_x(a), x = 1−3, as a function of proper reaction coordinate are shown in Figure S2 in Supporting Information. All optimized configurations of transition states for the reaction of H(g) + SiH_x(a) are given in Figure 6. Similar to the reaction of H(g) + Si_2H_5(a), four possible reaction mechanisms R6−R9 for the interaction of SiH_x(a) with H are considered, as alluded to in the introduction.

The likely H-abstraction mechanism begins by the attachment of a hydrogen atom at one of the hydrogen atoms in SiH_3(a), SiH_2(a), and SiH(a) through TS7, TS8, and TS9 to yield a H_2 molecule with SiH_2(a), SiH(a), and Si(a), respectively. The barriers at TS7, TS8, and TS9 are predicted to be 1.6, 3.3, and 7.0 kcal/mol, respectively. One should note that the very slight energy barrier of 1.6 kcal/mol may be neglected considering the thermal energy and within the expected calculation accuracy. The lengths of forming H···H bonds are calculated to be 1.557, 1.727, and 1.572 Å for TS7, TS8, and TS9, while the breaking H−Si bond distances are 1.528, 1.530, and 1.656 Å, respectively. The exothermicities of these processes are computed to be 48.5, 27.2, and 29.0 kcal/mol for the reactions of H(g) + SiH_3(a), H(g) + SiH_2(a), and H(g) + SiH(a), respectively.

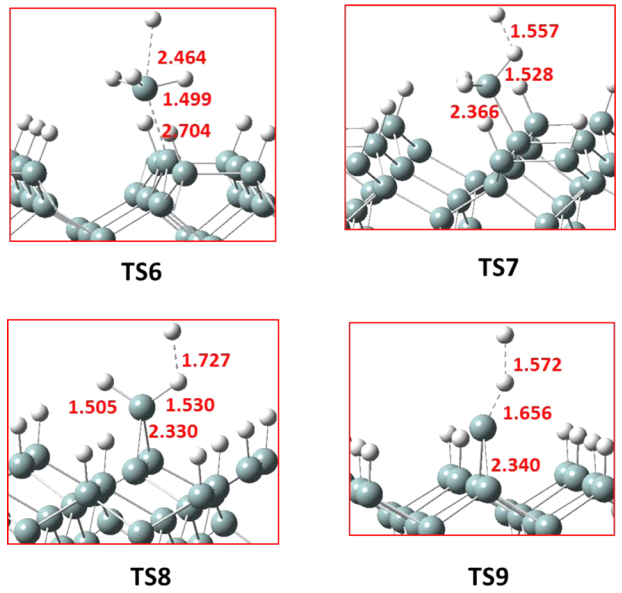

Figure 6. Optimized geometries of transition states for the reaction of H + SiH_x(a) (x = 1−3).

In addition, we also considered the other possible pathway via H-addition mechanism of H(g) + SiH_3(a) forming SiH_4(a). The energy barrier is evaluated to be 5.4 kcal/mol at TS6. In TS6, the forming H−Si and breaking Si−Si(s) bond distances are calculated to be 2.464 and 2.704 Å, respectively. This reaction process is evaluated to be exothermicity of 23.7 kcal/mol.

Rate Constant Calculations. On the basis of the above-mentioned PESs for the reactions of H(g) + Si_2H_5(a) and H(g) + SiH_3(a) on the H-covered Si(100)-(2 × 1) surface, we have calculated the rate constants for the reactions R1−R9 by the transition state theory as implemented in the VariFlex code.[72] The calculations have been performed in the temperature range of 200−3000 K using the TST and the computed rate constants (in units of cubic centimeters per molecule per second) represented by 3 parameters of modified Arrhenius expressions $k = AT^n \exp(-E_a/RT)$ are summarized in Table 3, together with the calculated rate constants at 300 and 500 K.

The rate constants for these reaction processes are described by[73]

$$d[X]_{surf}/dt = k(\theta/A_s)[X]_g$$

which has the units of a flux (molecules per square centimeter per second). In this formula, θ, A_s, and $[X]_g$ express the percentage of available surface sites, the area of the surface, and the concentration of Si_2H_5, SiH_3, and H gases in molecules per cubic centimeter, respectively. The kinetic results of this work may be used for simulation of Si_xH_y/H_2 based silicon thin-film growth by CVD processes.

dx.doi.org/10.1021/jp504612g | J. Phys. Chem. C 2014, 118, 20314−20322

Table 3. the Predicted Rate Expressions[a] for the Reactions R1−R9 in the Temperature Range of 200−3000 K with the Calculated Rate Constants at 300 and 500 K

reaction	A	m	E_a/R	T = 300 K	T = 500 K
$H(g) + Si_2H_5(a) \rightarrow H_2(g) + Si_2H_4(a)$	1.09×10^{-15}	1.58	3209.3	2.02×10^{-16}	3.26×10^{-14}
$H(g) + Si_2H_5(a) \rightarrow H_2(g) + SiHSiH_3(a)$	2.14×10^{-15}	1.37	1443.6	4.31×10^{-14}	5.97×10^{-13}
$H(g) + Si_2H_5(a) \rightarrow SiH_4(g) + SiH_2(a)$	1.48×10^{-15}	1.48	14073.9	2.90×10^{-32}	8.71×10^{-24}
$H(g) + Si_2H_5(a) \rightarrow 2SiH_3(a)$	1.79×10^{-13}	0.95	12224.6	8.11×10^{-29}	1.58×10^{-21}
$H(g) + Si_2H_5(a) \rightarrow Si_2H_6(g)$	7.14×10^{-19}	1.07	1463.6	2.42×10^{-18}	2.95×10^{-17}
$H(g) + SiH_3(a) \rightarrow SiH_4(g)$	2.2×10^{-15}	1.41	2496.98	1.66×10^{-15}	9.64×10^{-14}
$H(g) + SiH_3(a) \rightarrow H_2(g) + SiH_2(a)$	1.76×10^{-15}	1.55	123.84	8.05×10^{-12}	2.10×10^{-11}
$H(g) + SiH_2(a) \rightarrow H_2(g) + SiH(a)$	2.29×10^{-15}	1.38	1441.3	4.92×10^{-14}	6.80×10^{-13}
$H(g) + SiH(a) \rightarrow H_2(g) + Si(a)$	1.57×10^{-15}	1.43	3762.9	1.95×10^{-17}	6.12×10^{-15}

[a]Rate constants are represented by $k = AT^m \exp(-E_a/RT)$ in units of cubic centimeters per molecule per second.

CONCLUSIONS

The adsorption of Si_xH_y (x = 1−2; y = 1−5) species and the reaction of $H(g) + Si_xH_y$ species on the H-covered Si(100)-(2 × 1) surface have been elucidated by using the DFT calculations with spin-polarization effect. Our calculations show that it is easy to create the H vacancy sites and the dangling bonds by the SiH_3 and Si_2H_5 radicals on the H-covered Si(100) surface because of the low abstraction barriers (2.1 and 1.6 kcal/mol for SiH_3 and Si_2H_5 radicals, respectively). It was found that the Si_2H_6 and SiH_4 are assigned to be physisorption via molecular adsorption on the surface, whereas $Si_2H_5(a)$, $Si_2H_4(a)$, $SiHSiH_3(a)$, $SiH_3(a)$, $SiH_2(a)$, $SiH(a)$, and $Si(a)$ radicals interact more strongly with the surface. Potential energy surfaces for the reaction of $H(g) + Si_2H_5(a)$ and $H(g) + SiH_x(a)$ (x = 1−3) on the H-covered Si(100)-(2 × 1) surface were elucidated by implementing the NEB method. Calculation results show the hydrogen abstraction mechanisms of the reactions $H(g) + Si_2H_5(a)$ and $H(g) + SiH_3(a)$ may dominate on the H-covered Si(100)-(2 × 1) surface because of its low barrier and high exothermicity. The rate constants for the titular reactions were predicted by employing TST. The kinetic results may be important and can be applied for simulation of Si_xH_y/H_2 based Si-thin film growth by CVD processes, such as PECVD and Cat-CVD.

ASSOCIATED CONTENT

Supporting Information

Minimum energy pathways for the reactions of $H(g) + Si_2H_5(a)$ as the function of proper reaction coordinate (Figure S1); and minimum energy pathways for the reactions of $H(g) + SiH_x(a)$, x = 1−3, as the function of proper reaction coordinate (Figure S2). This material is available free of charge via the Internet at http://pubs.acs.org.

AUTHOR INFORMATION

Corresponding Author

*E-mail: htchen@cycu.edu.tw. Tel: +886-3-265-3324.

Notes

The authors declare no competing financial interest.

ACKNOWLEDGMENTS

The authors thank the Ministry of Economics and Ministry of Science and Technology, Taiwan, for supporting this study, under Contract 98-EC-17-A-07-S2-0043, NSC 101-2113-M-033-009-MY3, and MOST 103-2632-M-033-001-MY3 and the use of CPUs at the National Center for High-Performance Computing in Taiwan. In addition, we are deeply indebted to Professor M. C. Lin (from NCTU, Taiwan, and Emory University, U.S.A.) for persistent encouragement and instruction.

REFERENCES

(1) Matsuda, A. Thin-Film Silicon−Growth Process and Solar Cell Application. *Jpn. J. Appl. Phys., Part 1* **2004**, *43*, 7909−7920.
(2) Fuyuki, T.; Moriuchi, S.; Matsunami, H. Plasma anodic oxidation of indium phosphide. *Jpn. J. Appl. Phys., Part 1* **1983**, *22*, 1574−1576.
(3) Saitoh, T.; Muramatsu, S.; Shimada, T.; Migitaka, M. Optical and electrical properties of amorphous silicon films prepared by photochemical vapor deposition. *Appl. Phys. Lett.* **1983**, *42*, 678−679.
(4) Nishizaki, S.; Ohdaira, K.; Matsumura, H. Comparison of a-Si TFTs fabricated by Cat-CVD and PECVD methods. *Thin Solid Films* **2009**, *517*, 3581−3583.
(5) Schropp, R. E. I.; van der Werf, C. H. M.; Verlaan, V.; Rath, J. K.; Li, H. Ultrafast deposition of silicon nitride and semiconductor silicon thin films by hot wire chemical vapor deposition. *Thin Solid Films* **2009**, *517*, 3039−3042.
(6) Wang, Q. Hot-wire CVD amorphous Si materials for solar cell application. *Thin Solid Films* **2009**, *517*, 3570−3574.
(7) Jasinski, J. M.; Gates, S. M. Silicon chemical vapor deposition one step at a time: Fundamental studies of silicon hydride chemistry. *Acc. Chem. Res.* **1991**, *24*, 9−15.
(8) Pandey, S. C.; Singh, T.; Maroudas, D. Kinetic Monte Carlo simulations of surface growth during plasma deposition of silicon thin films. *J. Chem. Phys.* **2009**, *131*, 034503.
(9) Shah, A.; Torres, P.; Tscharner, R.; Wyrsch, N.; Keppner, H. Photovoltaic technology: The case for thin-film solar cells. *Science* **1999**, *285*, 692−698.
(10) Yang, D.; Ambo, K. S.; Holm-Kennedy, J. W. Four-color discriminating sensor using amorphous silicon drift-type photodiode. *Sens. Actuators* **1988**, *14*, 69−77.
(11) Xi, J.; Hollingsworth, R. E.; Buitrago, R. H.; Oakley, D.; Cumalat, J. P.; Nauenberg, U.; McNeil, J. A.; Anderson, D. F.; Perezmendez, V. Minimum ionizing particle detection using amorphous silicon diodes. *Nucl. Instrum. Methods Phys. Res., Sect. A* **1991**, *301*, 219−222.
(12) Matsumoto, K.; Koshi, M. Adsorption of disilyne [$Si(H_2)Si$] and disilene (H_2SiSiH_2) on the Si(100)-2 × 1 surface and on the H-terminated Si(100)-2 × 1 surface. *J. Electrochem. Soc.* **2008**, *155*, D419−D423.
(13) Abelson, J. R. Plasma deposition of hydrogenated amorphous silicon: Studies of the growth surface. *Appl. Phys. A.: Solids Surf.* **1993**, *56*, 493−512.
(14) Keudell, A. V.; Abelson, J. R. Direct insertion of SiH_3 radicals into strained Si-Si surface bonds during plasma deposition of hydrogenated amorphous silicon films. *Phys. Rev. B: Condens. Matter Mater. Phys.* **1999**, *59*, 5791−5798.
(15) Horvath, P.; Gallagher, A. Surface radicals in silane/hydrogen discharges. *J. Appl. Phys.* **2009**, *105*, 013304.

(16) Aketagawa, K.; Tatsumi, T.; Sakai, J. Limiting conditions of Si selective epitaxial growth in Si_2H_6 gas-source molecular beam epitaxy. *Appl. Phys. Lett.* **1991**, *59*, 1735−1736.
(17) Hirayama, H.; Tasumi, T.; Aizaki, N. Selective growth condition in disilane gas source silicon molecular beam epitaxy. *Appl. Phys. Lett.* **1988**, *52*, 2242−2243.
(18) Mokler, S. M.; Ohtani, N.; Xie, M. H.; Zhang, J.; Joyce, B. A. In Situ Observation of Growth-Rate Enhancement During Gas Source Molecular-Beam Epitaxy of $Si_{1-x}Ge_x$ Alloys on Si(100) Surfaces. *Appl. Phys. Lett.* **1992**, *61*, 2548−2550.
(19) Yamada, A.; Tanda, M.; Kato, F.; Konagai, M.; Takahashi, K. Gas source molecular-beam epitaxy of Si and SiGe using Si_2H_6 and GeH_4. *J. Appl. Phys.* **1991**, *69*, 1008−1012.
(20) Yoshinobu, T.; Nakayama, M.; Shiomi, H.; Fuyuki, T.; Matsunami, H. Atomic level control in gas source MBE growth of cubic SiC. *J. Cryst. Growth* **1990**, *99*, 520−524.
(21) Lin, D.-S.; Miller, T.; Chiang, T.-C. Adsorption and thermal reactions of disilane and the growth of Si films on Ge(100)-(2 × 1). *Phys. Rev. B: Condens. Matter Mater. Phys.* **1993**, *47*, 6543−6554.
(22) Price, R. W.; Tok, E. S.; Zhang, J. Probing the silane, disilane and germane adsorption kinetics on the silicon (0 0 1) surface. *J. Cryst. Growth* **2000**, *209*, 306−310.
(23) Shinohara, M.; Kimura, Y.; Saito, M.; Niwano, M. Infrared spectroscopy study of adsorption of silane on Si(0 0 1). *Surf. Sci.* **2002**, *502*, 96−101.
(24) Xia, L.-Q.; Jones, M. E.; Maity, N.; Engstrom, J. R. Dissociation and Pyrolysis of Si_2H_6 on Si Surfaces: The Influence of Surface Structure and Adlayer Composition. *J. Chem. Phys.* **1995**, *103*, 1691−1701.
(25) Gallagher, A. Some physics and chemistry of hot-wire deposition. *Thin Solid Films* **2001**, *395*, 25−28.
(26) Kawahara, T.; Tabuchi, N.; Arai, T.; Sato, Y.; Morimoto, J.; Mastumura, H. Coordination number constraint models for hydrogenated amorphous Si deposited by catalytic chemical vapour deposition. *J. Phys.: Condens. Matter* **2005**, *17*, S103−S110.
(27) Nakamura, S.; Matsumoto, K.; Susa, A.; Koshi, M. Reaction mechanism of silicon Cat-CVD. *J. Non-Cryst. Solids* **2006**, *352*, 919−924.
(28) Nozaki, Y.; Kitazoe, M.; Horii, K.; Umemoto, H.; Masuda, A.; Matsumura, H. Identification and gas phase kinetics of radical species in Cat-CVD processes of SiH_4. *Thin Solid Films* **2001**, *395*, 47−50.
(29) Nozaki, Y.; Kongo, K.; Miyazaki, T.; Kitazoe, M.; Horii, K.; Umemoto, H.; Masuda, A.; Matsumura, H. Identification of Si and SiH in catalytic chemical vapor deposition of SiH_4 by laser induced fluorescence spectroscopy. *J. Appl. Phys.* **2000**, *88*, 5437−5443.
(30) Tonokura, K.; Koshi, M. Reaction kinetics in silicon chemical vapor deposition. *Curr. Opin. Solid State Mater. Sci.* **2002**, *6*, 479−485.
(31) Aka, B.; Boch, E. Comparison of the processes induced by nitrogen dilution on the photodissociation of silane and disilane at 193 nm. *J. Photochem. Photobio., A* **2002**, *150*, 257−265.
(32) Matsuda, A.; Tanaka, K. Plasma spectroscopy—Glow discharge deposition of hydrogenated amorphous silicon. *Thin Solid Films* **1982**, *92*, 171−187.
(33) Kuwahara, T.; Ito, H.; Higuchi, Y.; Ozawa, N.; Kubo, M. Development of Crystal Growth Simulator Based on Tight-Binding Quantum Chemical Molecular Dynamics Method and Its Application to Silicon Chemical Vapor Deposition Processes. *J. Phys. Chem. C* **2012**, *116*, 12525−12531.
(34) Kuwahara, T.; Ito, H.; Kawaguchi, K.; Higuchi, Y.; Ozawa, N.; Kubo, M. Different Crystal Growth Mechanisms of Si(001)-(2 × 1):H during Plasma-Enhanced Chemical Vapor Deposition of SiH_3 and SiH_2 Radicals: Tight-Binding Quantum Chemical Molecular Dynamics Simulations. *J. Phys. Chem. C* **2013**, *117*, 15602−15614.
(35) Sriraman, S.; Agarwal, S.; Aydil, E. S.; Maroudas, D. Mechanism of hydrogen-induced crystallization of amorphous silicon. *Nature (London, U.K.)* **2002**, *418*, 62−65.
(36) Sriraman, S.; Valipa, M. S.; Aydil, E. S.; Maroudas, D. Hydrogen-induced crystallization of amorphous Si thin films. II. Mechanisms and energetics of hydrogen insertion into Si−Si bonds. *J. Appl. Phys.* **2006**, *100*, 053515.
(37) Valipa, M. S.; Sriraman, S.; Aydil, E. S.; Maroudas, D. Hydrogen-induced crystallization of amorphous silicon thin films. I. Simulation and analysis of film postgrowth treatment with H_2 plasmas. *J. Appl. Phys.* **2006**, *100*, 053514.
(38) Cereda, S.; Zipoli, F.; Bernasconi, M.; Miglio, L.; Montalenti, F. Thermal-Hydrogen Promoted Selective Desorption and Enhanced Mobility of Adsorbed Radicals in Silicon Film Growth. *Phys. Rev. Lett.* **2008**, *100*, 046105.
(39) Ceriotti, M.; Cereda, S.; Montalenti, F.; Miglio, L.; Bernasconi, M. Ab initio study of the diffusion and decomposition pathways of SiH_x species on Si(100). *Phys. Rev. B: Condens. Matter Mater. Phys.* **2009**, *79*, 165437.
(40) Chen, H.-T.; Hwang, C.-C.; Chiang, H.-J.; Chang, J.-G. Adsorption and Reaction of Si_2H_5 on Clean and H-Covered Si(100)-(2 × 1) Surfaces: A Computational Study. *J. Phys. Chem. C* **2011**, *115*, 15369−15374.
(41) Ng, R. Q. M.; Tok, E. S.; Kang, H. C. Molecular mechanisms for disilane chemisorption on Si(100)-(2 × 1). *J. Chem. Phys.* **2009**, *130*, 114702.
(42) Smardon, R. D.; Srivastava, G. P. Ab initio surface reaction energetics of SiH_4 and Si_2H_6 on Si(001)-(2 × 2). *J. Chem. Phys.* **2005**, *123*, 174703.
(43) Pandey, S. C.; Singh, T.; Maroudasa, D. On the growth mechanism of plasma deposited amorphous silicon thin films. *Appl. Phys. Lett.* **2008**, *93*, 151913.
(44) Kresse, G.; Furthmuller, J. Efficiency of ab-initio total energy calculations for metals and semiconductors using a plane-wave basis set. *Comput. Mater. Sci.* **1996**, *6*, 15−50.
(45) Kresse, G.; Hafner, J. Efficiency of ab-initio total energy calculations for metals and semiconductors using a plane-wave basis set. *Phys. Rev. B: Condens. Matter Mater. Phys.* **1993**, *47*, 558−561.
(46) Kresse, G.; Hafner, J. Ab initio molecular-dynamics simulation of the liquid-metal−amorphous-semiconductor transition in germanium. *Phys. Rev. B: Condens. Matter Mater. Phys.* **1994**, *49*, 14251−14269.
(47) Kresse, G.; Furthmuller, J. Efficient iterative schemes for ab initio total-energy calculations using a plane-wave basis set. *Phys. Rev. B: Condens. Matter Mater. Phys.* **1996**, *54*, 11169−11186.
(48) Perdew, J. P.; Burke, K.; Ernzerhof, M. Generalized Gradient Approximation Made Simple. *Phys. Rev. Lett.* **1996**, *77*, 3865−3868.
(49) Ceriotti, M.; Bernasconi, M. Diffusion and desorption of SiH_3 on hydrogenated H:Si(100)-(2 × 1) from first principles. *Phys. Rev. B: Condens. Matter Mater. Phys.* **2007**, *76*, 245309.
(50) Shi, J.; Tok, E. S.; Kang, H. C. The dissociative adsorption of silane and disilane on Si(100)-(2 × 1). *J. Chem. Phys.* **2007**, *127*, 164713.
(51) Henkelman, G.; Uberuaga, B. P.; Jönsson, H. A climbing image nudged elastic band method for finding saddle points and minimum energy paths. *J. Chem. Phys.* **2000**, *113*, 9901−9904.
(52) Mills, G.; Jönsson, H.; Schenter, G. Reversible work transition state theory: Application to dissociative adsorption of hydrogen. *Surf. Sci.* **1995**, *324*, 305−337.
(53) Glasstone, S.; Laidler, K. J.; Eyring, H. *The Theory of Rate Processes*; McGraw-Hill: New York, 1941.
(54) Kenichi, T.; Tetsuya, M.; Mitsuo, K. Formation Mechanism of Hydrogenated Silicon Clusters during Thermal Decomposition of Disilane. *J. Phys. Chem. B* **2002**, *106*, 555−563.
(55) Ruscic, B.; Berkowitz, J. Photoionization mass spectrometric studies of the transient species Si_2H_n (n = 2−5). *J. Phys. Chem.* **1991**, *95*, 2416−2432.
(56) Callomnon, J. H.; Hirota, E.; Kuchitsu, K.; Lafferly, W. J.; Maki, A. G.; Pote, C. S. *Structure Data on Free Polyatomic Molecules*; Landolt−Börnstein, New Series, Group 11;Springer-Verlag: Berlin, 1976; Vol. 7.
(57) Okada, Y.; Tokumaru, Y. Precise determination of lattice parameter and thermal expansion coefficient of silicon between 300 and 1500 K. *J. Appl. Phys.* **1984**, *56*, 314−320.

(58) Agarwal, S.; Sriraman, S.; Takano, A.; van de Sanden, M. C. M.; Aydil, E. S.; Maroudas, D. Mechanism and activation energy barrier for H abstraction by H(D) from a-Si:H surfaces. *Surf. Sci.* **2002**, *515*, L469.
(59) Agarwal, S.; Takano, A.; van de Sanden, M. C. M.; Maroudas, D.; Aydil, E. S. Abstraction of atomic hydrogen by atomic deuterium from an amorphous hydrogenated silicon surface. *J. Chem. Phys.* **2002**, *117*, 10805.
(60) Ramalingam, S.; Maroudas, D.; Aydil, E. S.; Walch, S. P. Abstraction of hydrogen by SiH_3 from hydrogen-terminated Si(001)-(2 × 1) surfaces. *Surf. Sci.* **1998**, *418*, L8−L13.
(61) Cereda, S.; Ceriotti, M.; Montalenti, F.; Bernasconi, M.; Miglio, L. Quantitative estimate of H abstraction by thermal SiH_3 on hydrogenated Si(001)(2 × 1). *Phys. Rev. B: Condens. Matter Mater. Phys.* **2007**, *75*, 235311.
(62) Bakos, T.; Valipa, M. S.; Maroudas, D. Thermally activated mechanisms of hydrogen abstraction by growth precursors during plasma deposition of silicon thin films. *J. Chem. Phys.* **2005**, *122*, 054703.
(63) Bakos, T.; Valipa, M.; Aydil, E. S.; Maroudas, D. Temperature dependence of precursor−surface interactions in plasma deposition of silicon thin films. *Chem. Phys. Lett.* **2005**, *414*, 61−65.
(64) Ramalingam, S.; Maroudas, D.; Aydil, E. S. Atomic-Scale Analysis of the Reactivity of Radicals from Silane/Hydrogen Plasmas with Silicon Surfaces. *Mater. Res. Soc. Symp. Proc.* **1998**, *485*, 107−112.
(65) Ramalingam, S.; Maroudas, D.; Aydil, E. S. Atomistic simulation study of the interactions of SiH_3 radicals with silicon surfaces. *J. Appl. Phys.* **1999**, *86*, 2872−2888.
(66) Kohler, H.-J.; Lischka, H. Bridged structures in multiply bonded silicon compounds: Disilyne, protonated disilyne and disilene. *Chem. Phys. Lett.* **1984**, *112*, 33−40.
(67) Onda, K.; Li, B.; Zhao, J.; Jordan, K. D.; Yang, J.; Petek, H. Wet Electrons at the H_2O/TiO_2(110). *Surf. Sci.* **2005**, *308*, 1154−1158.
(68) Huang, W.-F.; Chen, H.-T.; Lin, M. C. Density Functional Theory Study of the Adsorption and Reaction of H_2S on TiO_2 Rutile (110) and Anatase (101) Surfaces. *J. Phys. Chem. C* **2009**, *113*, 20411−20420.
(69) Chang, C.-Y.; Chen, H.-T.; Lin, M. C. Adsorption Configurations and Reactions of Nitric Acid on TiO_2 Rutile (110) and Anatase (101) surfaces. *J. Phys. Chem. C* **2009**, *113*, 6140−6149.
(70) Raghunath, P.; Lin, M. C. Adsorption Configurations and Reactions of Boric Acid on a TiO_2 Anatase (101) Surface. *J. Phys. Chem. C* **2008**, *112*, 8276−8287.
(71) Huang, W.-F.; Chen, H.-T.; Lin, M. C. Computational investigation of the adsorption and reactions of SiH_x (x = 0−4) on TiO_2 anatase (101) and rutile (110) surfaces. *Int. J. Quantum Chem.* **2013**, *113*, 1696−1708.
(72) Klippenstein, S. J.; Wagner, A. F.; Dunbar, R. C.; Wardlaw, D. M.; Robertson, S. H. *VariFlex*, Version 1.00 ed.; Argonne National Laboratory: Lemont, IL, 1999.
(73) Rettner, C. T.; Ashfold, M. N. R. *Dynamics of Gas-Surface Interaction*; Springer-Verlag: Berlin, 1991; Chapter 5.